KeAi
CHINESE ROOTS
GLOBAL IMPACT

Available online at www.sciencedirect.com

ScienceDirect

Advances in Climate Change Research 11 (2020) 227−238

www.keaipublishing.com/en/journals/accr/

Future sea level rise along the coast of China and adjacent region under 1.5 °C and 2.0 °C global warming

QU Ying[a], LIU Yonggang[a,*], Svetlana JEVREJEVA[b], Luke P. JACKSON[c]

[a] *Department of Atmospheric and Oceanic Sciences, School of Physics, Peking University, Beijing, 100871, China*
[b] *National Oceanography Center, Liverpool, L3 5DA, UK*
[c] *Programme for Economic Modelling, Nuffield College, Oxford University, OX1 1NF, UK*

Received 18 March 2020; revised 26 July 2020; accepted 2 September 2020
Available online 8 September 2020

Abstract

Although future sea level rise along the China coast has been projected by various studies for different representative concentration pathways (RCPs), the projections for different warming thresholds, e.g. 1.5 °C and 2.0 °C, have not been done specifically for this region, to the best of our knowledge. We provide such a projection here based on the climate projections of Coupled Model Intercomparison Project Phase 5 (CMIP5). The projections are given for 20 tide-gauge stations along the coast of China, Korea, Japan, and Vietnam. Vertical land motion (VLM) is also estimated for stations that have tide gauge records and satellite altimetry both covering the period of 1993−2018. Local land motion (LLM) is then estimated by subtracting the land motion due to glacial isostatic adjustment (GIA) from VLM. Without considering LLM, sea level rise by 2100 at median probability is projected to be 38−49 cm relative to the average sea level over 1986−2005 under warming of 1.5 °C, and increase to 46−57 cm when the warming threshold is increased to 2.0 °C. The steric component is the main contributor to this increase in sea level. Inclusion of LLM will not affect the sea level increase between the two warming thresholds, but it will make the local sea level rise by 2100 at certain locations substantially higher (up to 36 cm) or lower (up to 13 cm).

Keywords: Sea level rise; Coast of China; Tide gauge records; Vertical land motion; Warming of 1.5 °C; Warming of 2.0 °C

1. Introduction

More than 600 million people are living in the low-elevation coastal zone and the number may increase to more than one billion in 2060 (Neumann et al., 2015). The increase of future sea level under continuing global warming will threaten the lives and societies in these regions. In order to prepare for such situation, it is important to know how much sea level rise at each local region may be expected, e.g., near the end of this century, under different warming scenarios. Although it is widely recognized that global warming should be limited to 2.0 °C above preindustrial (1850−1900) level to avoid irreversible climate change risks (IPCC, 2018, 2019), some of the tipping points of the Earth system might be exceeded when global warming approaches 1.5 °C (Lenton et al., 2019). In that regard, the Paris Agreement (UNFCCC, 2015) in 2015 tried to pursue efforts to limit the future temperature rise to 1.5 °C in order to reduce the potential risks and impacts that will be caused by climate change (Jackson et al., 2018; Jevrejeva et al., 2018).

In hundred-year timescale, the global mean sea level rise consists of contributions from ocean expansion, glacier retreat, ice sheet melting, and land water storage reduction (Jackson and Jevrejeva, 2016). Compared to the global mean, the rises of regional sea level can be either much greater or much smaller due to local oceanic processes, land motion, or the change of gravitational potential due to mass redistribution (IPCC, 2013; Jevrejeva et al., 2016). During 1993−2018, coast of China have experienced faster sea level rise than the global

* Corresponding author.
E-mail address: ygliu@pku.edu.cn (LIU Y.).
Peer review under responsibility of National Climate Center (China Meteorological Administration).

https://doi.org/10.1016/j.accre.2020.09.001

mean (Nerem et al., 2018), and are more vulnerable to flooding associated with sea level rise than most coastal regions in the world given the large population and dense infrastructures along the coast (Han et al., 1995; Chen, 1997; Shi et al., 2000; Wu et al., 2003; Wang et al., 2012; Qu et al., 2018; Jevrejeva et al., 2018). It is, therefore, of vital importance to quantify the future sea level rise along the China coast, especially the gain in the reduction of sea level rise when the global warming target is lowered from 2.0 °C to 1.5 °C.

Future sea level rise projections can be made based on the climate projections by the Coupled Model Intercomparison Project Phase 5 (CMIP5) for different emission pathways. The methods for projecting future sea level rise can be classified into two categories: process-based (IPCC, 2013, 2014) and semi-empirical (e.g. Schaeffer et al., 2012). The former has been commonly used to project future regional and global sea level rise for different emission pathways (IPCC, 2013; Kopp et al., 2014; Jackson and Jevrejeva, 2016; Slangen et al., 2017), while the latter has been used to make global sea-level projection by 2300 for emission pathways that satisfy warming targets of 1.5 °C or 2.0 °C (Schaeffer et al., 2012; Nauels et al., 2017; Mengel et al., 2018). Using both methods, Jevrejeva et al. (2018) projected the global and regional sea level rise under global warming of 1.5 °C and 2.0 °C. They found that, at median probability, global mean sea level will rise up to 52 cm (depending on different temperature trajectories) by 2100 with a warming of 1.5 °C, while up to 63 cm with a warming of 2.0 °C. Using similar methods, Rasmussen et al. (2018) obtained 48 cm and 56 cm for warmings of 1.5 °C and 2.0 °C, respectively. The difference between Rasmussen et al. (2018) and Jevrejeva et al. (2018) is probably due to their different choice of climate-model data. In any case, there is significant reduction in sea level rise when warming threshold is changed from 2.0 °C to 1.5 °C.

Future sea level rise along the China coast has been projected for different emission pathways (Qu et al., 2018; Chen et al., 2018) and for different warming thresholds (Jevrejeva et al., 2018). The latter, however, did not take into account of the local land motion (LLM) and did not focus on the China coast specifically. By LLM, we mean land motions due to local processes that are not included in the glacial isostatic adjustment (GIA), such as underground water extraction, local tectonic movements etc. Rasmussen et al. (2018) obtained similar results to those in Jevrejeva et al. (2018), but focused on projecting the extreme sea levels under different global warming thresholds. Kopp et al. (2014) estimated the vertical land motion (VLM) using a statistical model and included in their sea-level projections. However, they used a single value for almost the whole China coast. Our main purpose here is to make future projections of sea level rise by 2100 along the China coast and nearby regions, such as Korea, Japan and Vietnam, for the global warming thresholds of 1.5 °C and 2.0 °C. In doing so, we take into consideration the influence of LLM at each of the tide-gauge stations. Before taking LLM into consideration, sea level rise at median probability by 2100 will be 38–49 cm and 46–57 cm under 1.5 °C and 2.0 °C warming respectively. After considering LLM, sea level rise by 2100 at certain locations will be subjected to substantial increase (up to 36 cm) or decrease (13 cm). We will also analyze the contribution from each component to the difference in sea level rises between the two warming thresholds. We find that steric component is the main contributor to future sea level rise at all locations at median probability under both warming scenarios.

2. Data and methods

2.1. Study area and tide gauge data

Here we select the regions located between 100° and 140°E and, 15°–40°N, which includes most part of the China coast and Korea coast, and part of the Japan and Vietnam coast (Fig. 1). Monthly tide gauge records for the selected 20 stations are downloaded from the Permanent Service for Mean Sea level (PSMSL) (Holgate et al., 2013; PSMSL, 2017). The records of all stations are longer than 40 years, among which 15 are between 50 and 60 years long, four are between 40 and 50 years long, and the NPQB station has the longest record of 69 years (detailed information are shown in the record of this last station is actually merged from stations North Point and Quarry Bay, because they have matching datum information (Ding et al., 2001).

The timespan of records and linear trend of sea level at each station are shown in Table 1. Here we estimate the trends and error bars with a simple linear regression model that includes an annual and semi-annual cycle. As the residuals of the model used to estimate the trends usually have serial correlation, which will cause underestimation of the true standard error, we adjust the standard error by reducing the degree of freedom (Dangendrof et al., 2014), following an autoregressive model of order 1. Sea level trends of all stations along the China coast show great spatial differences, varying from 0.8 ± 1.1 to 5.5 ± 0.4 mm per year (Table 1).

2.2. Satellite altimetry data and sea level pressure data

There is no Global Positioning System (GPS) data open to the public in Mainland China, so the monthly satellite altimetry data provided by AVISO (Archiving, Validation, and Interpretation of Satellite Oceanographic Data) are used here in combination with the tide gauge records to estimate the VLM trends. The monthly mean sea level anomalies measured by satellite altimetry covering the period 1993–2018 are provided by AVISO. They have interpolated the along-track data onto a 0.25° × 0.25° grid. Because the satellite altimetry gives sea surface height relative to the reference ellipsoid, while the tide gauge recorded sea surface height is relative to a benchmark that is influenced by VLM, the difference between the two can give us an estimate of the VLM trends at each station where GPS observations are not available (Kuo et al., 2004; Chen et al., 2018; Wöppelmann and Marcos, 2016; Qu et al., 2018). We also check the reliability of our estimates of VLM by comparing them to those provided by Système

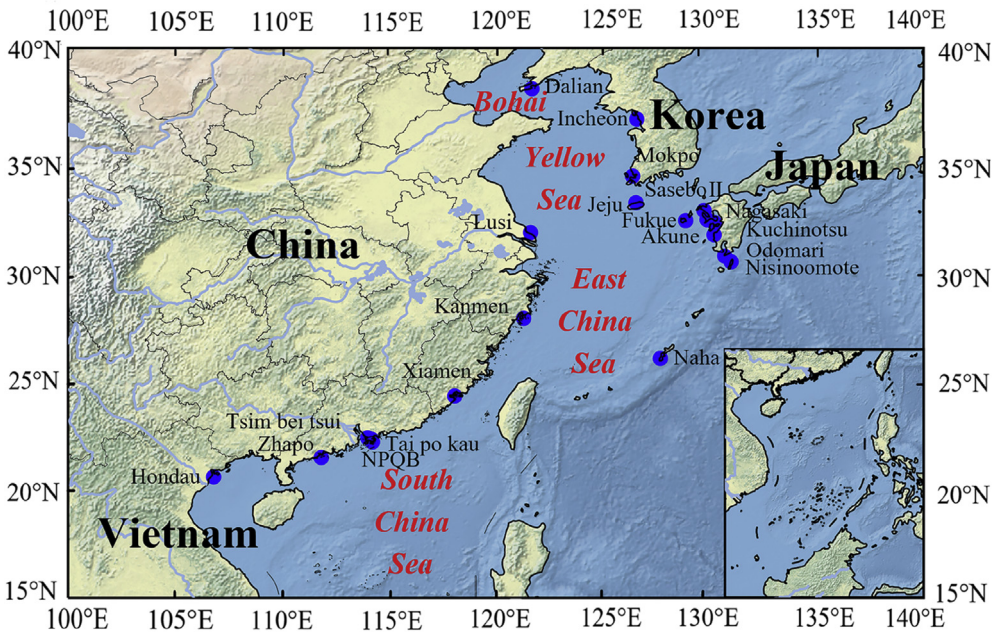

Fig. 1. The spatial distribution of selected tide-gauge stations within the study area.

d'Observation du Niveau des Eaux Littorales (SONEL: www.sonel.org), which were calculated using similar method except that the satellite altimetry data had a lower spatial resolution (1° × 1°). The limitations of this indirect method of estimating the VLM have been discussed in previous studies (e.g. Kleinherenbrink et al., 2018).

As the sea level anomalies from AVISO have been corrected for inverse barometer effects using the sea level pressure (SLP) data, we need to correct all the tide gauge records in the same way. The SLP data from NCEP/NCAR Reanalysis datasets are used for this purpose (Kalnay et al., 1996).

2.3. Probabilistic sea-level projections by 2100

Compared to global mean sea-level change, regional sea-level change is more complex due to spatially non-uniform temperature and salinity changes and mass addition or subtraction. All these changes induce additional non-uniform sea-level changes through deformation of the solid Earth and the geoid; such effect is considered through the so-called 'fingerprints' (Jackson and Jevrejeva, 2016; Jevrejeva et al., 2018). Following Jackson and Jevrejeva (2016), regional sea-level projection is calculated by combining all the sea-level components using a probability density function (PDF) method:

where all F functions on the right-hand side (RHS) are fingerprints associated with their respective triggering term. For example, $F_{\mathrm{SAL}}(\theta,\phi)$ is the fingerprint for considering the effect of self-attraction and loading (SAL) induced by steric sea-level change $STR(\theta,\phi,t)$. $GLA(t)$, $ANT(t)$, $GRE(t)$ and $LAN(t)$ are mass changes of glaciers, Antarctic Ice Sheet, Greenland Ice Sheet and land water storage, respectively. $GIA(\theta,\phi)\cdot t$ is the sea-level change due to continuous glacial isostatic adjustment induced by deglaciation since 22,000 years ago. Here we assume all the sea level components are uncorrelated, and a single fingerprint for the Antarctic Ice Sheet is adopted for which a specific relationship between mass loss from West Antarctic and East Antarctic is assumed (Bamber and Aspinall, 2013; Jackson and Jevrejeva, 2016). Note that by 'steric' we mean 'sterodynamic' which includes both the steric and dynamic sea-level changes, as commonly used in the literature.

Though there are no representative concentration pathways (RCP) in CMIP5 specifically designed to limit warming by 2100 to below 1.5 °C and 2.0 °C, the 5%–95% range of warming for RCP2.6 is between 0.19 and 2.31 °C and for RCP4.5 it is between 1.62 and 3.21 °C relative to pre-industrial levels. These warmings are close to the temperature targets of 1.5 °C and 2.0 °C. Jevrejeva et al. (2018) identified those model experiments in CMIP5 whose

$$RSL(\theta,\phi,t) = F_{\mathrm{SAL}}(\theta,\phi)\cdot STR(\theta,\phi,t) + F_{\mathrm{GLA}}(\theta,\phi)GLA(t) + GIA(\theta,\phi)\cdot t$$
$$+F_{\mathrm{ANT}}(\theta,\phi)\cdot ANT(t) + F_{\mathrm{GRE}}(\theta,\phi)\cdot GRE(t) + F_{\mathrm{LW}}(\theta,\phi)\cdot LAN(t) \quad (1)$$

Table 1
The timespan of sea level records and the calculated linear trend with their 95% confidence interval at all selected tide-gauge stations (The last column shows the linear trend corrected for VLM (vertical land motion), which is calculated only for the period 1993−2018).

Station	Lon (°E)	Lat (°N)	Country	Time span	Linear trend (mm per year)	Linear trend corr. for VLM (mm per year)
Dalian	121.68	38.87	China	1970−2018	3.5 ± 0.4	2.8 ± 0.4
Lusi	121.62	32.13	China	1967−2018	5.5 ± 0.4	2.3 ± 0.4
Kanmen	121.28	28.08	China	1959−2018	2.4 ± 0.3	1.4 ± 0.3
Xiamen	118.07	24.45	China	1954−2004	1.1 ± 0.6	N/A
Tsim bei tsui (HK)	114.01	22.49	China	1974−2018	0.8 ± 1.1	1.8 ± 1.1
Tai po kau (HK)	114.18	22.44	China	1963−2018	3.3 ± 0.6	3.9 ± 0.6
NPQB (HK)	114.21	22.30	China	1950−2018	1.3 ± 0.4	2.8 ± 0.4
Zhapo	111.82	21.58	China	1959−2018	2.4 ± 0.4	2.8 ± 0.4
Incheon	126.59	37.45	Korea	1960−2018	1.4 ± 0.5	3.3 ± 0.5
Mokpo	126.38	34.78	Korea	1960−2018	3.8 ± 0.5	0.6 ± 0.5
Jeju	126.54	33.53	Korea	1964−2018	5.2 ± 0.4	3.1 ± 0.4
Sasebo II	129.72	33.16	Japan	1966−2018	2.2 ± 0.4	2.2 ± 0.4
Nagasaki	129.87	32.74	Japan	1965−2018	2.6 ± 0.4	1.9 ± 0.4
Fukue	128.85	32.70	Japan	1965−2018	1.5 ± 0.4	2.1 ± 0.4
Kuchinotsu	130.20	32.61	Japan	1975−2018	3.2 ± 0.5	2.6 ± 0.5
Akune	130.19	32.02	Japan	1970−2018	1.4 ± 0.4	1.3 ± 0.4
Odomari	130.69	31.02	Japan	1965−2018	2.0 ± 0.5	1.8 ± 0.5
Nisinoomote	130.99	30.74	Japan	1965−2018	2.4 ± 0.4	2.4 ± 0.4
Naha	127.67	26.21	Japan	1966−2018	2.2 ± 0.6	2.7 ± 0.6
Hondau	106.80	20.67	Vietnam	1957−2013	2.1 ± 0.5	N/A
Mean					2.6 ± 0.5	2.3 ± 0.5

temperature increase averaged over 2080−2100 were within ±0.21 and ± 0.28 °C of the warming targets 1.5 °C and 2.0 °C, respectively, and obtained 16 and 23 model experiments for the two warming targets, respectively. Besides the steric sea level components from CMIP5 model outputs, all other individual sea level components have also been projected or included. The fingerprints of glaciers, Greenland Ice Sheet (GIS) and Antarctic Ice Sheet (AIS) were from Bamber and Riva, (2010); sea-level projection contributed by the surface mass balance in 19 glacial regions are estimated following Marzeion et al. (2012); the contribution of AIS surface mass balance is estimated following Fettweis et al. (2013), while GIS surface mass balance is estimated following de Vries et al. (2014); the sea-level projection contributed by the ice sheet dynamic are from IPCC AR5 (IPCC, 2013); the sea-level change due to land water storage was from Wada et al. (2012); the sea-level change due to past glacial−interglacial cycles, i.e. the glacial isostatic adjustment (GIA), is independent of the emission pathways and was obtained from the ICE 6G _C (VM5a) model (Peltier et al., 2015).

The data above have been collected by Jevrejeva et al. (2018) and here we use the same data to estimate the probabilistic sea-level projections by 2100 along the China coast and nearby regions, with the influence of LLM considered in addition. To project the sea level, we first derive a Burr PDF (Burr, 1942) specific to each sea-level component at each time slice, then we sample the PDF randomly 1000 times to get 1000 realizations of each component. The realizations are then substituted in Eq. (1) to get 1000 realizations of the total sea level. More details can be found in Jackson and Jevrejeva (2016).

3. Results

3.1. Vertical land motion

VLM is an important source of local sea-level changes and can contaminate the tide gauge records. It may be caused by several geophysical processes such as local tectonic movements, earthquakes, groundwater extraction, and GIA (IPCC, 2013; Peltier et al., 2015). Because the VLM induced by GIA can be estimated independently by GIA models, it is subtracted from the total VLM estimated from the differences between the satellite altimetry (AL) and tide gauge (TG) records to obtain LLM. The LLM is calculated for 18 stations whose tide gauge records cover the period 1993−2018, the altimetry era.

The VLM rates are between −3.2 ± 1.8 and 1.9 ± 0.8 mm per year (Table 2). Along the China coast, the three stations to the north of 28°N, i.e., Dalian, Lusi and Kanmen, are all subsiding and the four stations to the south, i.e., Tsim bei tsui, Tai po Kau, NPQB and Zhapo, are all uplifting. The Lusi station subsides at the fastest rate, −3.2 ± 0.9 mm per year and the other two northern stations subside at rates at or slightly slower than −1 mm per year. The southern stations all uplift at moderate rates, between 0.4 ± 0.6 and 1.5 ± 1.2 mm per year. The study area as a whole does not have the pattern of subsiding in the north and uplifting in the south; for the stations outside China, Mokpo, Jeju, Nagasaki, Kuchinotsu, Akune and Odomari are subsiding and Incheon, Fukue and Naha are uplifting. Lusi, Mokpo and Jeju stations are geographically near each other and all have large sinking rates (Table 2), may be speculated to be due to the same tectonic process.

Table 2
Sea level linear trend from tide gauge records and satellite altimetry over 1993−2018 (unit: mm per year), at 95% confidence interval.

Station	Trend from TG	Trend from AL	VLM trend (AL-TG)	VLM trend from SONEL	GIA trend	LLM trend
Dalian	4.2 ± 0.8	3.6 ± 0.8	−0.7 ± 0.6	−0.8 ± 0.4	0.44	−1.1 ± 0.6
Lusi	6.2 ± 1.1	3.0 ± 1.0	−3.2 ± 0.9	−2.6 ± 0.8	0.53	−3.7 ± 0.9
Kanmen	4.7 ± 1.2	3.8 ± 1.1	−1.0 ± 0.8	−1.3 ± 0.5	0.45	−1.4 ± 0.8
Tsim bei tsui	2.3 ± 1.8	3.4 ± 1.0	1.0 ± 1.6	0.4 ± 0.6	0.43	0.6 ± 1.6
Tai po kau	2.9 ± 1.4	3.5 ± 1.0	0.6 ± 1.3	0.1 ± 0.5	0.41	0.2 ± 1.3
NPQB	2.0 ± 1.4	3.5 ± 1.1	1.5 ± 1.2	N/A	0.40	1.1 ± 1.2
Zhapo	2.9 ± 1.2	3.3 ± 1.0	0.4 ± 0.6	0.8 ± 0.5	0.46	−0.1 ± 0.6
Incheon	2.6 ± 1.0	4.5 ± 0.9	1.9 ± 0.8	2.0 ± 0.6	0.56	1.3 ± 0.8
Mokpo	6.0 ± 1.6	2.8 ± 1.0	−3.2 ± 1.8	N/A	0.51	−3.7 ± 1.8
Jeju	5.7 ± 0.9	3.6 ± 0.9	−2.1 ± 0.7	−4.6 ± 0.3	0.39	−2.5 ± 0.7
Sasebo II	4.0 ± 1.0	4.1 ± 0.9	0.0 ± 0.5	−0.5 ± 0.3	0.44	−0.4 ± 0.5
Nagasaki	4.2 ± 1.0	3.5 ± 0.9	−0.7 ± 0.5	−1.0 ± 0.3	0.41	−1.2 ± 0.5
Fukue	2.6 ± 0.9	3.2 ± 0.8	0.6 ± 0.4	0.5 ± 0.3	0.32	0.3 ± 0.4
Kuchinotsu	3.6 ± 1.0	3.0 ± 0.8	−0.6 ± 0.6	−0.7 ± 0.3	0.42	−1.1 ± 0.6
Akune	2.9 ± 0.9	2.8 ± 0.8	−0.1 ± 0.5	−0.3 ± 0.3	0.34	−0.4 ± 0.5
Odomari	3.6 ± 1.2	3.3 ± 1.1	−0.2 ± 0.9	−1.1 ± 0.5	0.22	−0.4 ± 0.9
Nisinoomote	3.4 ± 1.0	3.4 ± 1.1	0.0 ± 0.6	−0.3 ± 0.3	0.18	−0.2 ± 0.6
Naha	2.8 ± 1.5	3.3 ± 1.6	0.5 ± 0.3	0.3 ± 0.2	0.10	0.4 ± 0.3
Mean	3.7 ± 1.2	3.4 ± 1.0	−0.3 ± 0.8	N/A	0.39	−0.7 ± 0.8

Notes: [a] Tide Gauge; [b] Altimetry; [c] VLM trends estimation from SONEL over 1993−2014; [d] ICE-6G_C_VM5a model (Peltier et al., 2015); [e] Local Land Motion (LLM), calculated by VLM minus GIA; [f] VLM trends over 1993−2013.

Compared to GIA, which has a smooth variation between 0.1 and 0.56 mm per year (ICE-6G_C_VM5a model; Peltier et al., 2015), the VLM rates show a much larger spatial variation (Table 2). As a result, the LLM also exhibits a large spatial variation, between −3.7 ± 1.8 and 1.3 ± 0.8 mm per year. Assuming VLM trends calculated for the period 1993−2018 remain the same over the whole observational period, the SLC rates for the 18 tide-gauge stations are corrected for VLM. The spatially averaged SLC rate is 2.6 ± 0.5 mm per year and 2.3 ± 0.5 mm per year before and after correction, respectively (Table 1).

According to our estimates above, the LLM rates are generally much greater than GIA and contribute a large fraction to the past sea-level changes at a few stations. However, it is uncertain how the LLM will change in the future. Here we assume that the LLM rate at each tide-gauge station remains the same for 2019−2100 as that over 1993−2018. The contribution to the projected sea-level changes at year 2100 by LLM at each station is presented in Fig. 2. The values vary between −13 to 36 cm, certainly not negligible if local sea-level projections are to be made properly.

3.2. Future sea-level projection in 2100 under warming of 1.5 °C and 2.0 °C

Table 3 shows the projected sea level in 2100 relative to 1986−2005 for the 20 stations at the median (50%), 5% and 95% probabilities under warming of 1.5 °C and 2.0 °C over the period of 2080−2100. The effect of LLM is not included in the numbers in Table 3. From the table we can see that under warming of 1.5 °C, the sea-level changes are between 14 and 22 cm, 38−49 cm, and 61−75 cm at 5%, 50% and 95% probabilities, respectively. Under warming of 2.0 °C, the corresponding sea-level changes become 21−28 cm, 46−57 cm, and 72−86 cm, respectively, a quite large increase. When the warming target is relaxed from 1.5 °C to 2.0 °C, the mean sea level rise averaged over all stations increases by 6, 6 and 10 cm for the 5%, 50% and 95% probabilities, respectively, and the sea level rises for the median probability will increase by 8 cm at 6 of the 20 stations, 7 cm at 7 of them, 6 cm at 5 of them, and 5 cm at the rest 2. Dalian station has the smallest projected sea level rise across 20 stations for both warming scenarios while Naha has the highest.

The spatial pattern of sea level rise for the 1.5 °C warming scenario is shown in Fig. 3. Clearly, the Bohai Sea and Yellow Sea experience less sea level rise than other regions. When the warming limit is relaxed from 1.5 °C to 2.0 °C, the relative changes in Bohai Sea are the largest, reaching approximately 50%, 23% and 18% for projections at 5%, 50% and 95% probabilities, respectively (Fig. 3). The relative changes in sea level rise become smaller moving towards Southern China and Vietnam. This means that Northern China, western coast of Korea will be impacted relatively more severely when the warming target is relaxed from 1.5 °C to 2.0 °C.

The sea-level changes in 2100 are relatively smooth across all stations when the LLM is not considered (Table 3). When the LLM is added into the future sea-level projection, the spatial variability increases substantially (Fig. 4); the projected sea level rises at median probability could be larger than 80 cm at Lusi and Mokpo while less than 40 cm at Incheon. Because LLM is not dependent on the warming scenarios, inclusion of LLM into sea-level projections also changes the ratios in Fig. 3 considerably since it affects the denominator but not the numerator. For example, the projected sea level rise (at median probability) at Lusi station for warming threshold of 2.0 °C is 17% larger than that for warming threshold of 1.5 °C before LLM is taken into account, but it is reduced to

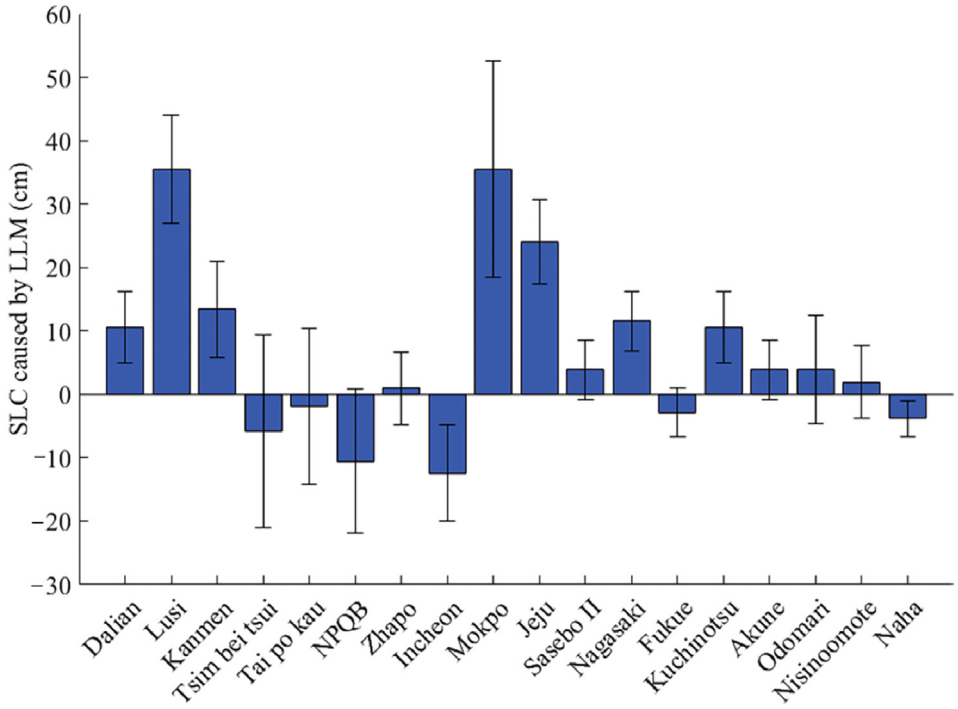

Fig. 2. Sea level change (SLC) caused by local land motion (LLM) at 2100 at each station.

9% when LLM is taken into account; for the Incheon station, the ratio increases from 17% to 24%.

3.3. Contributors to rising sea levels

The projection of total as well as component sea level rise for the median probability at Dalian is shown in Fig. 5 as an example. Some components have nonlinear variations with time at this location, but the rankings of their contribution to total sea level rise remain the same for the whole period from 2010 to 2100. The main contributor to the future sea level rise at this station is the steric component under both warming scenarios, and the second largest contributor is the glacier melting. Under warming of 1.5 °C, the contribution of the steric component is only slightly larger than that of the glaciers, while under warming of 2.0 °C, the former becomes much larger than the latter. The third and fourth contributors to the sea level rise are the melting of the Greenland ice sheet and the Antarctic ice sheet. Land water storage has negligible contribution to the total sea level rise. Opposite to the other contributors, GIA is a negative contributor to future sea level rise.

Table 3
Projected sea level rise at 2100 relative to 1986–2005 for different probabilities at each station (unit: cm; effect of LLM is not included in these numbers).

Station	1.5 °C			2.0 °C		
	5%	50%	95%	5%	50%	95%
Dalian	14	38	61	21	46	72
Lusi	16	41	65	22	48	74
Kanmen	20	46	71	26	53	81
Xiamen	17	42	67	22	49	77
Tsim bei tsui	19	45	69	25	51	78
Tai po kau	19	45	69	25	51	78
NPQB	19	45	69	25	51	78
Zhapo	19	45	70	25	51	78
Incheon	17	42	66	23	49	76
Mokpo	17	42	66	23	50	76
Jeju	18	44	69	24	51	78
Sasebo II	18	44	69	22	49	77
Nagasaki	18	44	69	22	49	77
Fukue	18	44	69	23	51	78
Kuchinotsu	18	44	69	22	49	77
Akune	19	46	72	25	54	82
Odomari	19	46	72	26	54	83
Nisinoomote	19	46	72	26	54	83
Naha	22	49	75	28	57	86
Hondau	18	42	66	23	49	75
Mean	18	44	68	24	50	78

The relative contributions of components to the total sea level rise at other stations in the study area are quite similar to those at Dalian. Contributions of all components to future sea level rise in 2100 for 1.5 °C and 2.0 °C warming scenarios at median probability for all tide-gauge stations are presented in Fig. 6. The steric component is the largest and the glacier component the second largest contributor to total sea level rise for almost all tide-gauge stations, the only exception is the Hondau station at which the glacier has a larger contribution than the steric component for the 1.5 °C warming scenario (Fig. 6a). From this figure, it can be seen that Dalian station has a smaller sea level rise than all other stations for the 1.5 °C warming scenario because of its small steric, glacier and land-water-storage components. However, its steric component increases a lot when the warming limit is relaxed to 2.0 °C, catching up with those at other stations. The large sea level rise at Akune, Odomari, Nisinoomote and Naha stations for

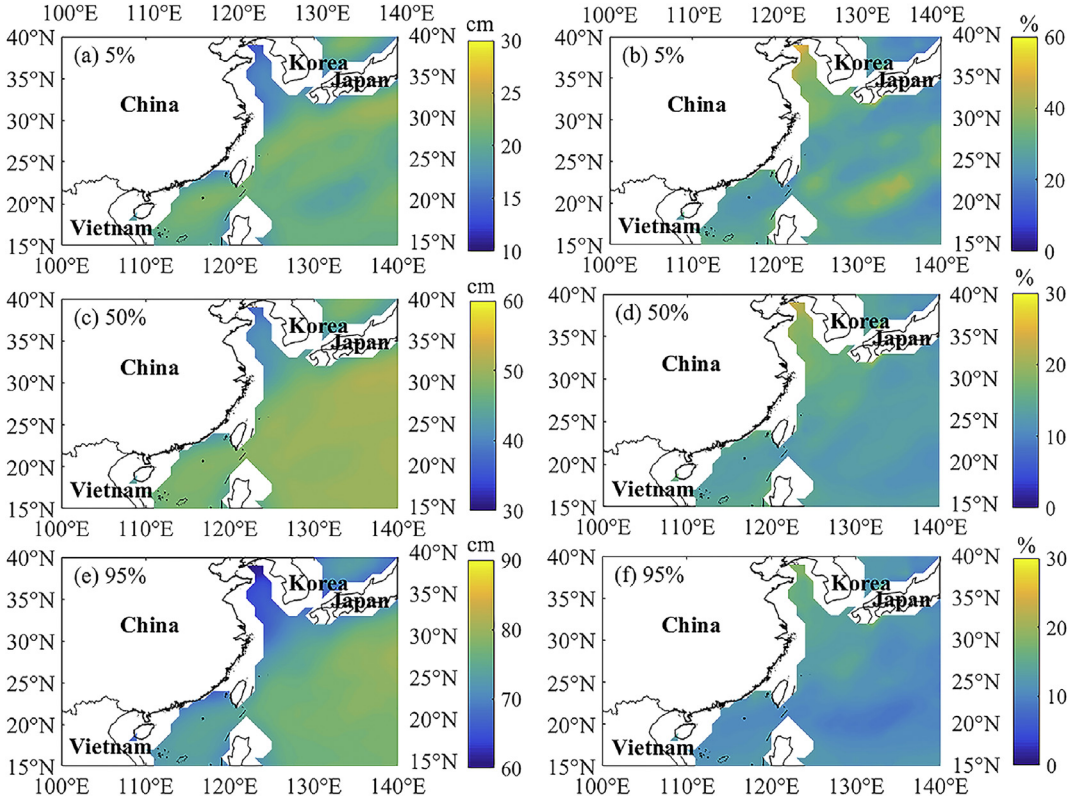

Fig. 3. The left column (a,c,e) are the projected sea level rise at 2100 relative to 1986–2005 under warming of 1.5 °C; the right column (b, d,f) are the relative changes in sea level rise between warmings of 2.0 °C and 1.5 °C.

the 2.0 °C warming scenario are mainly due to the large steric component and small (negative) GIA component (Fig. 6b).

Neither the LLM nor the GIA contributes to the difference in sea level rise between warming thresholds of 1.5 °C and 2.0 °C, while all the other components contribute to this difference. The fractions of contribution of each component at all stations for the median probability projection are presented in Fig. 7. Consistent with the ranking of component contributions to the

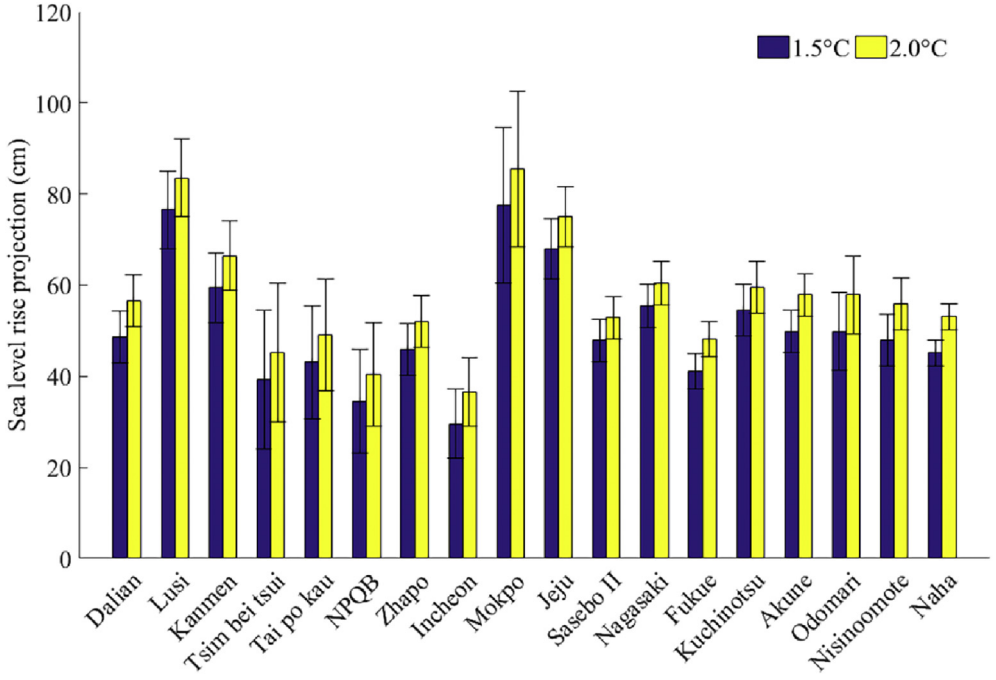

Fig. 4. Projected sea level rise in 2100 relative to 1986–2005 at median probability (50%) for each station (The local land motion has been taken into account).

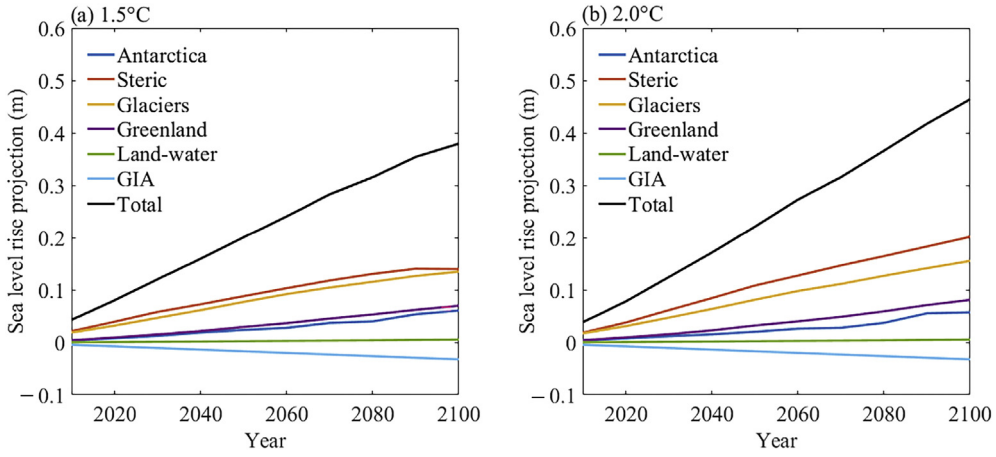

Fig. 5. Future total and component sea-level rise projections for Dalian station at median (50%) probability relative to 1986–2005 for (a) 1.5 °C and (b) 2.0 °C warming scenarios.

total sea level rise under both warming scenarios, the steric component, the glacier retreating and GIS melting remain the top three contributors to the difference in sea level rise between the two warming scenarios. The change in mass balance of GIS contributes positively to future sea level rise with warming from 1.5 °C to 2.0 °C due to the increase in ablation that outweighs increase in accumulation associated with snowfall. However, when the warming target is relaxed from 1.5 °C to 2.0 °C, the mass loss of AIS may decrease (for the timescale of interest here) and contributes negatively to the sea level rise. In the 21st century, the ablation of AIS is projected to be small due to the low surface temperature that inhibits surface melting, except the areas close to the coast and on the Peninsula (Ligtenberg et al., 2013), making the increase in snowfall within its extensive interior area dominant (Krinner et al., 2007; Uotila et al., 2007; Bracegirdle et al., 2008).

The projected total as well as component sea level rise averaged over the China coast is shown in Fig. 8 for all three probabilities and both warming scenarios. The ranking of component contributions to the total sea level rise for the median probability projections (Fig. 8b and e) are similar to that in Fig. 5, where the results for a single station is shown. Unsurprisingly, the GIA has a negative contribution in all cases in Fig. 8. The contributions of both land-water storage and AIS change from negative values in the 5% probability projection to positive values in the 95% probability projection, reflecting the very poor agreement among models in predicting the evolution of these two components, especially the AIS. The steric component remains the largest contributor to sea level rise as in Fig. 5, except in the 5% probability projection where the mass loss from glaciers has the largest contribution (Fig. 8a and d).

4. Discussion

4.1. Uncertainties in local land motion and future sea-level projection

The VLM or LLM in this study is estimated from the difference in the rates of sea level measured by satellite altimeter and tide gauge during the period of 1993–2018. The estimated rates of VLM have a large spatial variability, and vary between -3.2 ± 1.8 and 1.9 ± 0.8 mm per year among all stations. In China, Lusi subsides at the fastest rate of 3.2 ± 0.9 mm per year. Lusi is located in the Yangtze River Delta, underground water extraction together with the local sandy environment can cause severe subsidence (Ren, 1993). The rates of VLM at about half of the stations are similar in magnitude to the rate of global mean sea level rise, therefore, should be estimated accurately in order to get reliable future local sea level rise. Unfortunately, the error in the estimated VLM is hard to estimate using another independent method due to lack of relevant GPS data in mainland China. However, studies in other regions have shown that this indirect VLM estimation method gives reasonable results (e.g., Kleinherenbrink et al., 2018). Our estimation of VLM is overall consistent with those estimated by Qu et al. (2018) and Chen et al. (2018) with the same method for slightly shorter periods, 1993–2016 and 1993–2012, respectively.

How LLM will change in the future is an important question for which there is still no good answer. Tectonic processes are on million-year timescale, so its influence on rate of SLC might be treated as constant on hundred-year timescale. The sediment compaction may also be considered to be a relatively stable process on hundred-year timescale. However, the earthquake and groundwater extraction are hard to predict for the future. This uncertainty in LLM causes uncertainty in the projected future sea level rise.

The projection of other sea level components relies on climate projections by CMIP5 models, and estimation of ice losses from glaciers and ice sheets. These could all have large uncertainties as have been widely discussed previously (IPCC, 2013; Kopp et al., 2014; Jackson and Jevrejeva, 2016; Jevrejeva et al., 2016; Qu et al., 2018), and give the large range of sea level rise between projections for 5% and 95% probabilities. Moreover, the CMIP5 as well as the newly available CMIP 6 model experiments are not designed specifically to achieve warming targets of 1.5 °C and 2.0 °C. The uncertainties can be narrowed down when more model results are

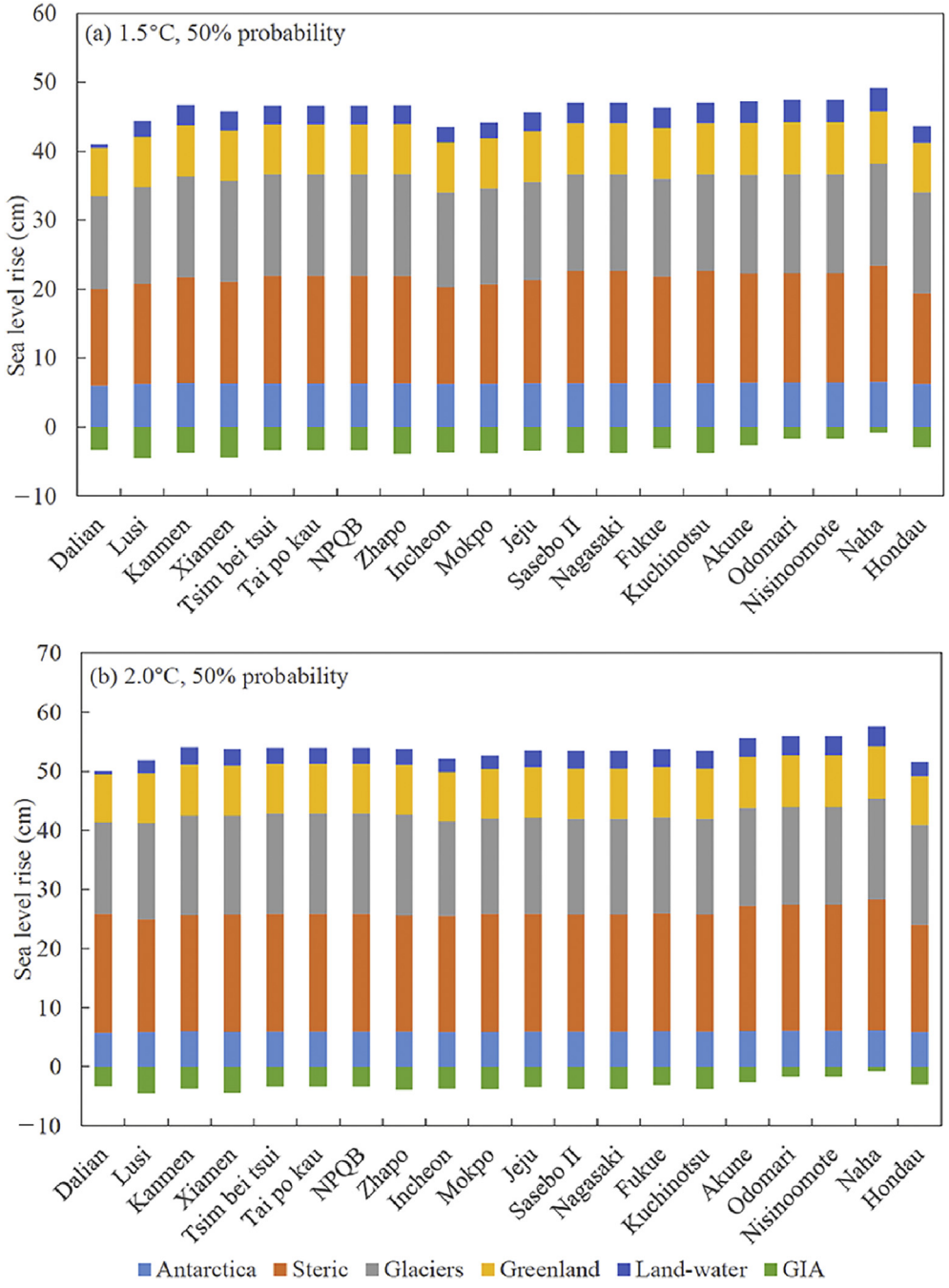

Fig. 6. The contributions of all components to sea level rise in 2100 relative to 1986–2005 for (a) 1.5 °C and (b) 2.0 °C warming scenarios at median probability.

available, especially those designed for the same purpose as pursued here. Our next step will be to incorporate the model data from CMIP6.

4.2. Potential risks under the two warming scenarios

Coastal sea level rise can cause the increasing potential risks of several hazards including shore-line erosion, wetland inundation, and coastal flooding during storm events, which have significant influences on the enormous number of coastal communities around the world (Passeri et al., 2015). Jevrejeva et al. (2018) made use of the Dynamic Interactive Vulnerability Assessment (DIVA) modelling framework to compute the impact of future sea level rise, and found that China will pay for the largest cost of flooding under warming of 1.5 °C, which is one order of magnitude larger than those paid by Japan and the USA. With warming increased from 1.5 °C to 2.0 °C, the changes in sea level rise could result in an increase in annual cost of 0.4 trillion USD for China (Jevrejeva et al., 2018). However, their estimate was based on sea level rise without including the influence of LLM. As shown here, the LLM is spatially highly variable and is large at certain locations. Therefore, the economic cost due to sea level rise may need to be re-estimated in the future.

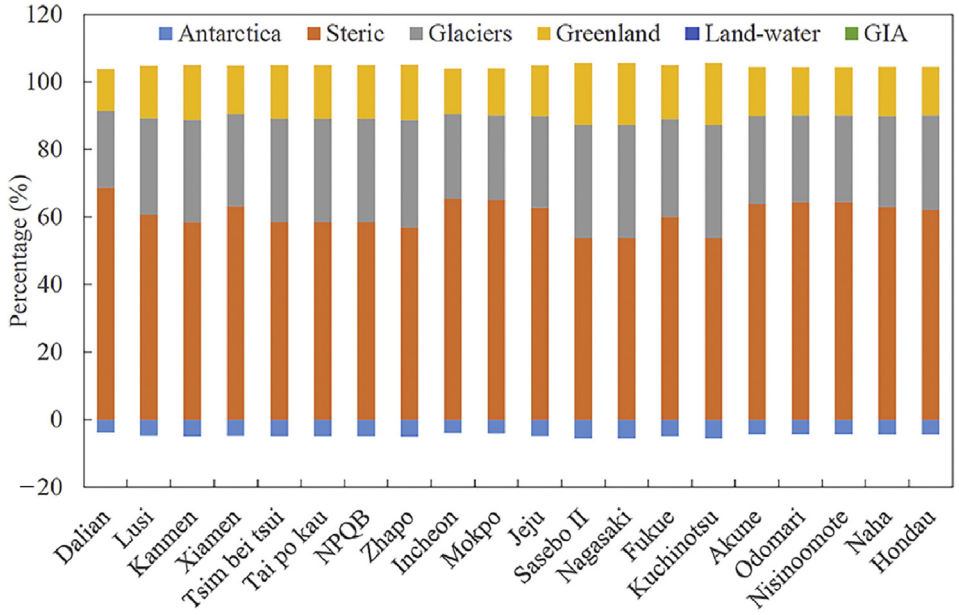

Fig. 7. The fractional contributions of all components to the difference in sea level rise in 2100 relative to 1986−2005 between warming scenarios of 2.0 °C and 1.5 °C. The example shown here is for the median probability (The numbers add up to 100% for each column; the contribution of Antarctic Ice Sheet at warming of 2.0 °C is negative compared that at warming of 1.5 °C (light blue bar at the bottom of each column)).

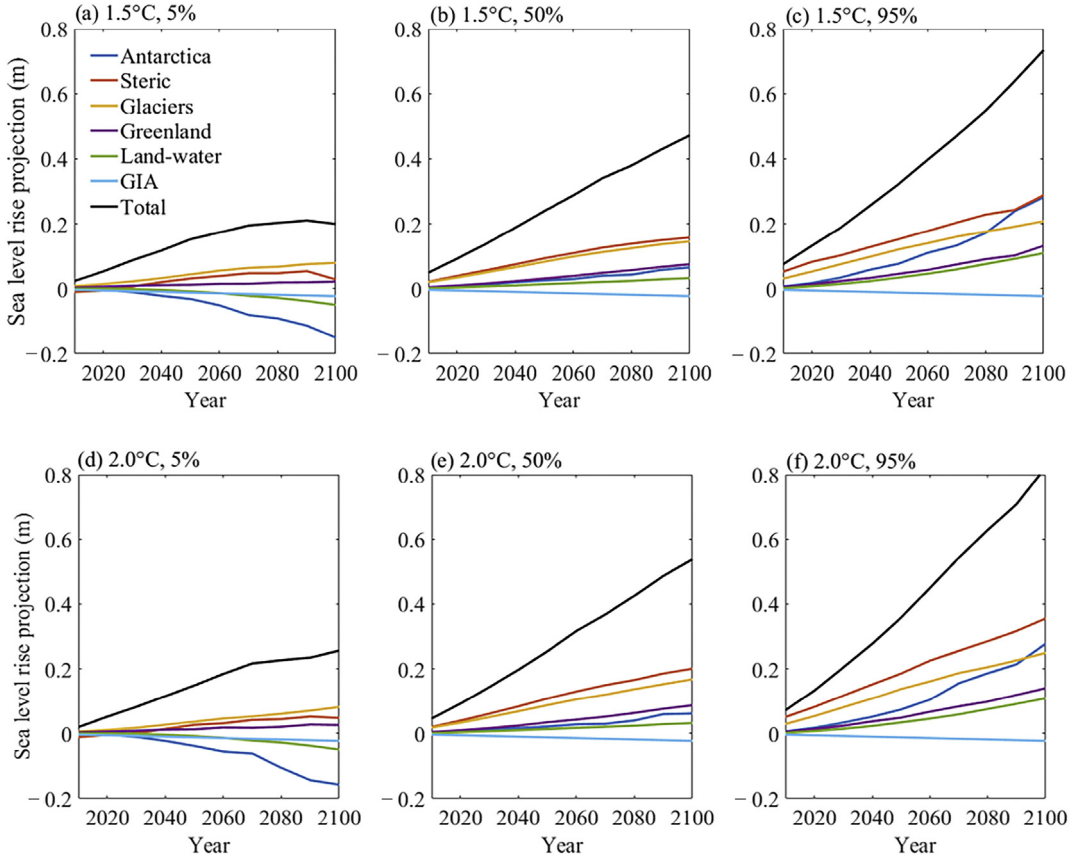

Fig. 8. Projected total and component sea level rise by 2100 relative to 1986−2005 averaged over the China coast for 5%, 50% and 95% probabilities under warming scenarios of 1.5 °C and 2.0 °C.

5. Conclusions

We project the total sea level rise by 2100 as well as the contributions from each component at 20 tide-gauge stations along or near China coast under warmings of both 1.5 °C and 2.0 °C. Especially, the LLM at each station, an important contribution to local sea level rise, is also estimated. Before LLM is taken into account, the future sea level rises relative to the average sea level over 1986−2005 at 5%, 50% and 95% probabilities are [14, 22] cm, [38, 49] cm and [61, 75] cm in 2100, respectively, if the warming is limited to 1.5 °C, but will increase to [21, 28] cm, [46, 57] cm and [72, 86] cm, respectively, if the warming threshold is increased to 2.0 °C. The projected sea level rise does not differ greatly across stations within the study area. The LLM, although does not affect the increase in sea level between the two warming scenarios, can have a large impact on the projected sea level rise under each of the warming scenarios at certain locations. For example, for a median probability projection under warming of 1.5 °C, an additional rise of sea level by 36 cm at stations Lusi and Mokpo and a reduced rise of sea level by 13 cm at station Incheon will be caused by LLM.

For the median probability projections under both warming scenarios, the steric component is the largest contributor to future sea level rise at all stations. The second to fourth largest contributors are the glaciers, GIS and AIS. Change of land water storage contributes little to the total sea level rise. GIA makes a negative contribution to future sea level rise in the whole region. Steric is also by far the largest contributor to the increased sea level rise when the threshold of warming is changed from 1.5 °C to 2.0 °C, and is followed by the contribution of the glaciers and GIS.

Declaration of competing interest

The authors declare no conflict of interests.

Acknowledgments

This work is supported by the Chinese MOST (2017YFA0603801). We thank three anonymous reviewers and the editor whose comments and recommendations improved our article greatly. We are gratefully for the help of Zhao Zhou-Qiao and Guo Anboyu on producing the maps used herein.

References

Bamber, J.L., Aspinall, W.P., 2013. An expert judgement assessment of future sea level rise from the ice sheets. Nat. Clim. Change 3, 424−427. https://doi.org/10.1038/NCLIMATE1778.

Bamber, J.L., Riva, R.E.M., 2010. The sea level fingerprint of recent ice mass fluxes. Cryosphere 4, 621−627. https://doi.org/10.5194/tc-4-621-2010.

Bracegirdle, T.J., Connolley, W.M., Turner, J., 2008. Antarctic climate change over the twenty first century. J. Geophys. Res. Atmos. 113, D03103. https://doi.org/10.1029/2007JD008933.

Burr, I.W., 1942. Cumulative frequency functions. Ann. Math. Stat. 13 (2), 215−232. http://www.jstor.org/stable/2235756.

Chen, J., 1997. The impact of sea level rise on China's coastal areas and its disaster hazard evaluation. J. Coast Res. 2050, 925−930.

Chen, N., Han, G.-Q., Yang, J.-S., 2018. Mean relative sea level rise along the coasts of the China Seas from mid-20th to 21st centuries. Continent. Shelf Res. 152, 27−34. https://doi.org/10.1016/j.csr.2017.12.002.

d.Vries, H., Katsman, C., Drijfhout, S., 2014. Constructing scenarios of regional sea level change using global temperature pathways. Environ. Res. Lett. 9 (11), 115007. https://doi.org/10.1088/1748-9326/9/11/115007.

Dangendrof, S., Calafat, F.M., Arns, A., et al., 2014. Mean sea level variability in the North Sea: processes and implications. J. Geophys. Res. Oceans. 119 (10), 1022−1037. https://doi.org/10.1002/2013JC009415.

Ding, X., Zheng, D., Chen, Y., et al., 2001. Sea level change in Hong Kong from tide gauge measurements of 1954-1999. J. Geodyn. 74, 683−689. https://doi.org/10.1007/s001900000128.

Fettweis, X., Franco, B., Tedesco, M., et al., 2013. Estimating the Greenland ice sheet surface mass balance contribution to future sea level rise using the regional atmospheric climate model. MAR. Cryosphere 7, 469−489. https://doi.org/10.5194/tc-7-469-2013.

Han, M., Hou, J., Wu, L., 1995. Potential impacts of sea level rise on China's coastal environment and cities: a national assessment. J. Coast Res. (14), 79−95.

Holgate, S.J., Matthews, A., Woodworth, P.L., et al., 2013. New data systems and products at the permanent service for mean sea level. J. Coast Res. 29 (3), 493−504. https://doi:10.2112/JCOASTRES-D-12-00175.1.

IPCC, 2013. Climate Change 2013: The Physical Science Basis. Contribution of Working Group I to the Fifth Assessment Report of the Intergovernmental Panel on Climate Change. Cambridge University Press, Cambridge and New York.

IPCC, 2014. Climate Change 2014: Impacts, Adaptation, and Vulnerability. Part A: Global and Sectoral Aspects. Contribution of Working Group II to the Fifth Assessment Report of the Intergovernmental Panel on Climate Change. Cambridge University Press, Cambridge and New York.

IPCC, 2018. Global warming of 1.5°C An IPCC special report on the impacts of global warming of 1.5 °C above pre-industrial levels and related global greenhouse gas emission pathways, in the context of strengthening the global response to the threat of climate change, sustainable development, and efforts to eradicate poverty. https://www.ipcc.ch/site/assets/uploads/sites/2/2019/05/SR15_SPM_version_report_LR.pdf.

IPCC, 2019. Special report on the ocean and cryosphere in a changing climate. https://www.ipcc.ch/site/assets/uploads/sites/3/2019/12/SROCC_FullReport_FINAL.pdf.

Jackson, L.P., Jevrejeva, S., 2016. A probabilistic approach to 21st century regional sea-level projections using RCP and High-end scenarios. Global Planet. Change 146, 179−189. https://doi.org/10.1016/j.gloplacha.2016.10.006.

Jackson, L.P., Grinsted, A., Jevrejeva, S., 2018. 21st century sea level rise in line with the Paris Accord. Earth's Future 6 (2), 213−229. https://doi.org/10.1002/2017EF000688.

Jevrejeva, S., Jackson, L.P., Riva, R.E.M., et al., 2016. Coastal sea level rise with warming above 2 °C. Proc. Natl. Acad. Sci. Unit. States Am. 113 (47), 11342−13347. https://doi.org/10.1073/pnas.1605312113.

Jevrejeva, S., Jackson, L.P., Grinsted, A., et al., 2018. Flood damage costs under the sea level rise with warming of 1.5 °C and 2 °C. Environ. Res. Lett. 13 (7), 074014 https://doi.org/10.1088/1748-9326/aacc76.

Kalnay, E., Kanamitsu, M., Kistler, R., et al., 1996. The NCEP/NCAR 40-year reanalysis project. Bull. Am. Meteorol. Soc. 77, 437−470.

Kleinherenbrink, M., Riva, R.E.M., Frederikse, T., 2018. A comparison of methods to estimate vertical land motion trends from GNSS and altimetry at tide gauge stations. Ocean Sci. 14, 187−204. https://doi.org/10.5194/os-14-187-2018.

Kopp, R.E., Horton, R.M., Little, C.M., et al., 2014. Probabilistic 21st and 22nd century sea-level projections at a global network of tide-gauge sites. Earth's Future 2 (8), 383−406. https://doi:10.1002/2014EF000239.

Krinner, G., Magand, O., Simmonds, I., et al., 2007. Simulated Antarctic precipitation and surface mass balance at the end of the twentieth and twenty-first centuries. Clim. Dynam. 28, 215−230.

Kuo, C.Y., Shum, C.K., Braun, A., et al., 2004. Vertical crustal motion determined by satellite altimetry and tide gauge data in Fennoscandia. Geophys. Res. Lett. 31 (1), L01608. https://doi.org/10.1029/2003GL019106.

Lenton, T.M., Rockström, J., Gaffney, O., et al., 2019. Climate tipping points-too risky to bet against. Nature 575, 592−595. https://doi.org/10.1038/d41586-019-03595-0.

Ligtenberg, S.R.M., Berg, W.J.v.d., Broeke, M.R.v.d., et al., 2013. Future surface mass balance of the Antarctic ice sheet and its influence on sea level change, simulated by a regional atmospheric climate model. Clim. Dynam. 41, 867−884. https://doi.org/10.1007/s00382-013-1749-1.

Marzeion, B., Jarosch, A.H., Hofer, M., 2012. Past and future sea-level change from the surface mass balance of glaciers. Cryosphere 6, 1295−1322. https://doi.org/10.5194/tc-6-1295-2012.

Mengel, M., Nauels, A., Rogelj, J., et al., 2018. Committed sea level rise under the Paris agreement and the legacy of delayed mitigation action. Nat. Commun. 9, 601. https://doi: 10.1038/s41467-018-02985-8.

Nauels, A., Rogelj, J., Schleussner, C.F., et al., 2017. Linking sea level rise and socioeconomic indicators under the shared socioeconomic pathways. Environ. Res. Lett. 12, 114002. https://doi: 10.1088/1748-9326/aa92b6.

Nerem, R.S., Beckley, B.D., Fasullo, J.T., et al., 2018. Climate-change-driven accelerated sea level rise detected in the altimeter era. Proc. Natl. Acad. Sci. Unit. States Am. 115 (9), 2022−2025. https://doi.org/10.1073/pnas.1717312115.

Neumann, B., Vafeidis, A.T., Zimmermann, J., et al., 2015. Future coastal population growth and exposure to sea level rise and coastal flooding-a global assessment. PloS One 10 (3), e0118571. https://doi.org/10.1371/journal.pone.0118571.

Passeri, D.L., Hagen, S.C., Medeiros, S.C., et al., 2015. The dynamic effects of sea level rise on low-gradient coastal landscapes: a review. Earth's Future 3 (6), 159−181. https://doi.org/10.1002/2015EF000298.

Peltier, W.R., Argus, D.F., Drummond, R., 2015. Space geodesy constrains ice age terminal deglaciation: the global ICE-6G C (VM5a) model. J. Geophys. Res. Solid Earth. 120 (1), 450−487. https://doi.org/10.1002/2014JB011176.

PSMSL (Permanent Service for Mean Sea level), 2017. Tide gauge data. http://www.psmsl.org/data/obtaining/.

Qu, Y., Jevrejeva, S., Jackson, L.P., et al., 2018. Coastal sea level rise around the China Seas. Global Planet. Change 172, 454−463. https://doi:10.1016/j.gloplacha.2018.11.005.

Rasmussen, D.J., Bittermann, K., Buchanan, M.K., et al., 2018. Extreme sea level implications of 1.5 °C, 2.0 °C, and 2.5 °C temperature stabilization targets in the 21st and 22nd centuries. Environ. Res. Lett. 13 (3), 034040 https://doi.org/10.1088/1748-9326/aaac87.

Ren, M.-E., 1993. Relative sea level changes in China over the last 80 years. J. Coast Res. 9 (1), 229−241. http://www.jstor.org/stable/4298080.

Schaeffer, M., Hare, W., Rahmstorf, S., et al., 2012. Long-term sea level rise implied by 1.5 ˚C and 2 ˚C warming levels. Nat. Clim. Change 2, 867−870. https://www.nature.com/articles/nclimate1584.

Shi, Y.-F., Zhu, J.-W., Xie, Z.-R., et al., 2000. Prediction and prevention of the impacts of sea level rise on the Yangtze River Delta and its adjacent areas. Science in China (Series D) 43 (4), 412−422.

Slangen, A.B.A., Adloff, F., Jevrejeva, S., et al., 2017. A review of recent updates of sea-level projections at global and regional scales. Surv. Geophys. 38, 385−406. https://doi.org/10.1007/s10712-016-9374-2.

UNFCCC, 2015. The Paris Agreement. Decision 1/CP.21.

Uotila, P., Lynch, A., Cassano, J.J., et al., 2007. Changes in Antarctic net precipitation in the 21st century based on Intergovernmental Panel on Climate Change (IPCC) model scenarios. J. Geophys. Res. Atmos. 112, D10107. https://doi.org/10.1029/2006JD007482.

Wada, Y., van Beek, L.P.H., Weiland, F.C.S., et al., 2012. Past and future contribution of global groundwater depletion to sea level rise. Geophys. Res. Lett. 39 (9), L09402. https://doi.org/10.1029/2012GL051230.

Wang, J., Gao, W., Xu, S.-Y., et al., 2012. Evaluation of the combined risk of sea level rise, land subsidence, and storm surges on the coastal areas of Shanghai, China. Climatic Change 115, 537−558. https://doi.org/10.1007/s10584-012-0468-7.

Wöppelmann, G., Marcos, M., 2016. Vertical land motion as a key to understanding sea level change and variability. Rev. Geophys. 54, 64−92. https://doi:10.1002/2015RG000502.

Wu, Q., Zheng, X.-X., Xu, H., et al., 2003. Relative sea-level rising and its control strategy in coastal regions of China in the 21st century. Sci. China, Ser. A 46 (1), 74−83.